Structural diversity and photo-physical and magnetic properties of dimeric to 1D polymeric coordination polymers of lighter lanthanide(III) dinitrobenzoates

A.K. Jassal, B.S. Sran, Yan Suffren, Kevin Bernot, Fabrice Pointillart, O. Cador, G. Hundal

Structural Diversity, Photo-physical and Magnetic Properties of Dimeric to 1D Polymeric Coordination Polymers of Lighter Lanthanide(III) Dinitrobenzoates

Amanpreet Kaur Jassal,[a] Balkaran Singh Sran,[a] Yan Suffren,[b] Kevin Bernot,[b] Fabrice Pointillart*,[c] Olivier Cador*,[c] Geeta Hundal* [a]

Single crystal diffraction studies reveal the formation of the following 10 new complexes of lighter Ln(III) ions of general formula $\{[Ln(\mu_2\text{-}\mathbf{L1})_3.(H_2O)_2].H_2O\}_n$ (Ln = Nd (**1**), Eu (**2**)), $[Nd(\mu_2\text{-}\mathbf{L2})_2.(CH_3COO).(H_2O)_2]_n$ (**3**), $[Ln_2(\mu_2\text{-}\mathbf{L2})_5.(\mathbf{L2}).(H_2O)_4]_n$ (Ln = Sm (**4**), Ce (**5**), Pr (**6**)), $[La_2(\mu_2\text{-}\mathbf{L2})_6.(H_2O)_3.(DMF)]_n$ (**7**) (DMF = dimethylformamide), $[Ln(\mu_2\text{-}\mathbf{L2})_2.(\mathbf{L2}).(H_2O)_3]_2$ (Ln = Eu (**8**), Gd (**9**)) and $[Gd(\mathbf{L2}).(CH_3COO)_2.(H_2O)_2]_2$ (**10**), where **L1** and **L2** stand for anions of 3,5- and 2,4-dinitrobenzoic acid. Complexes **1**-**7** are 1D coordination polymers while **8**-**10** are dinuclear complexes. The luminescence properties of Nd(III) and Eu(III) analogues displayed metal-centred emission with **L1** exhibiting weak but more efficient sensitization than **L2**. A study of the magnetic properties of compounds gave a clear demonstration of field-induced Single Ion Magnet behaviour of the Nd(III) compounds **1** & **3**. Their behaviour has been compared to the previously reported analogous Nd(III) complexes and role of lattice solvent and polymorphism on magnetic behaviour has been observed.

Introduction

Over the past years, the coordination polymers (CPs) containing lanthanides have become highly relevant due to their fascinating,[1,2] unique physico-chemical properties and potential applications ranging from biomedical analysis to materials science[1-8] as optical, electronic and catalytic materials and molecular-based magnets.[9-13] A typical electronic structures entrusted upon lanthanides allow them to have a wide range of luminescence (NIR to UV) and magnetic (isotropic to anisotropic) properties.[14] For the synthesis of polymeric complexes of 4*f* metal ions with diverse coordination behavior,[15-16] choice of appropriate organic ligands with versatile functional groups or use of secondary building blocks is highly effective.[17-19] In this context, carboxylate ligands are hard Lewis bases and are well known to strongly bind Ln(III) ions as compared to other. In particular, when aromatic carboxylic acids are employed as antenna ligands, the coordinated lanthanide ions exhibit higher luminescent stabilities than other organic ligands.[20-22] Recently, some lanthanide benzoate or salicylate complexes with strong luminescence and intriguing structural features have been reported in literature.[23-28] Mostly aromatic carboxylate ligands were selected considering the fact that the carboxylate groups interact strongly with the oxophilic lanthanide ions and the delocalized π systems provide strongly absorbing chromophore.[29] On the other hand, the presence of an electron-withdrawing group dramatically decreases the overall sensitization efficiency of the Ln(III)-centred luminescence due to dissipation of the excitation energy by means of a π*-n transition of the $-NO_2$ substituent along with the participation of the ILCT bands. The weaker photoluminescence of some Ln(III) complexes is attributable to the poor match of the triplet energy levels of nitro benzoic acid derivatives with that of the emitting level of lanthanide metal ion.

The lanthanides, that are key ingredients of hard magnets[30] have become the latest craze in the world of molecular magnets as SMMs (single molecule magnets), SCMs (single chain magnets) or SIMs (single ion magnets)), for the past two decades.[31-39] Strong magnetic moment and high magnetic anisotropy of these ions coupled with crystal field symmetry and electronic distribution of ligands, play strong role in generation and fine-tuning of the properties of SMMs. The literature shows that the association of carboxylate-based ligands and lanthanide ions could lead to the observation of slow magnetic relaxation due to the appropriate electrostatic distribution in the proximity of the magnetic ion.[40-46]

The most popular lanthanides to design SMMs are the heavier ions such as Dy(III), Tb(III) and Er(III),[41-54] notwithstanding the fact that that lighter ions such as Ce(III), Pr(III) and Nd(III) have been recently used as elaborated SMMs.[55-62] The latter, however suffer from weak spin-orbit coupling and thus the isolation of molecular magnets among them is a relatively less visited arena.[63-68] Picking up from there, we report here the synthesis, spectroscopic characterization, crystal structure determination, thermal, luminescence and magnetic properties of complexes of aromatic carboxylates, **L1H** (3,5-dinitrobenzoic acid) and **L2H** (2,4-dinitrobenzoic acid) ligands with first half series of Ln(III) elements, up to Gd(III). Though all complexes (except for La(III)) have interesting photo-physical

[a] *Department of Chemistry, UGC sponsored centre of advance studies-II, Guru Nanak Dev University, Amritsar-143005, Punjab, India.*
[b] *Institut des Sciences Chimiques de Rennes, UMR 6226 CNRS-Université de Rennes 1, 263 Avenue du Général Leclerc, 35042 Rennes Cedex, France.*
[c] *Institut des Sciences Chimiques de Rennes, UMR CNRS 6226, INSA Rennes, 20 Avenue des buttes de Coesmes, 35708 Rennes, France.*

Electronic Supplementary Information (ESI) available: structural information, thermal analysis, emission spectra and static magnetic measurements. CCDC No.s for complexes (**1**-**10**) are **1584543**-**52** .See DOI: 10.1039/x0xx00000x

and magnetic properties, an exhibit of slow magnetic relaxation under an optimal applied magnetic field brings the two Nd(III) complexes among the rare examples of Nd(III)-based luminescent compounds with SMM behaviour.

Experimental Section

Materials and physical measurements

All the reagents were commercially available and used as received. C, H, N elemental analyses were obtained with a CHNS-O analyser flash-EA-1112 series. The IR spectra of compounds were recorded on Perkin ELMER FTIR spectrometer in the range 4000-400 cm^{-1}. Thermo gravimetric analysis (TGA) data were collected on a NetzschTG-209 instrument. UV spectra were recorded on a Shimadzu 1700 spectrophotometer in DMSO. The solid emission and excitation spectra were measured using a Horiba-Jobin Yvon Fluorolog-3® spectrofluorimeter, equipped with a three slit double grating excitation and emission monochromator with dispersions of 2.1 nm/mm (1200 grooves/mm). The steady-state luminescence was excited by unpolarized light from a 450 W xenon CW lamp and detected at a 90° angle by a Hamamatsu R928 photomultiplier tube for the visible (sensitivity 190-860 nm) and a diode InGaAs for the infrared (sensitivity 800-1800 nm). Spectra were reference corrected for both the excitation source light intensity variation (lamp and grating) and the emission spectral response (detector and grating). Appropriate filters were used to remove the residual excitation laser light, the Rayleigh scattered light and associated harmonics from spectra. The emission/excitation spectra recordings were realized on powder samples introduced in cylindrical quartz cells of 0.7 cm diameter and 2.4 cm height, which were placed directly inside an integrating sphere. The dc magnetic susceptibility measurements were performed on solid polycrystalline sample with a Quantum Design MPMS-XL SQUID magnetometer between 2 and 300 K in an applied magnetic field of 1 kOe in the 2-20 K temperature range and 10 kOe between 20 and 300 K. These measurements were all corrected for the diamagnetic contribution as calculated with Pascal's constants[69]. Magnetization measurements in alternating field a various frequencies have been performed with 3 Oe oscillating field amplitude. The X-ray powder diffraction (XRPD) measurements were made on Bruker D8 Focus X-ray diffractometer with CuKα radiation (λ =1.54056 Å).

General Procedure

General Procedure for synthesis of complexes NdL1 (1), NdL2(ac) (3) and GdL2ac (10). L1H or **L2H** (1 mmol, 0.21 g) was suspended in a moderate volume of acetonitrile. To an aqueous solution of $Nd(CH_3COO)_3.H_2O$ (0.342 g, 1 mmol) or $Gd(CH_3COO)_3.xH_2O$ (0.334 g, 1 mmol), 0.1 N NaOH was added drop wise and the solution was stirred well. The solution of **L1H** or **L2H** was added to this solution drop wise and the resulting solution was allowed to slowly evaporate to give pink colour crystals for **NdL1 (1)**, **NdL2(ac) (3)** and colourless crystals for **GdL2ac (10)**. M.p.>300 ºC.

General Procedure for synthesis of complexes EuL1(2), SmL2(4), CeL2(5), PrL2(6), LaL2(7), EuL2(8) and **GdL2(9). L1H** or **L2H** (1 mmol, 0.21 g) was suspended in a moderate volume of acetonitrile (20 mL). To an aqueous solution of metal nitrate (1 mmol), (i.e. $Eu(NO_3)_3.5H_2O$, $Sm(NO_3)_3.6H_2O$, $La(NO_3)_3.xH_2O$, $Ce(NO_3)_3.xH_2O$, $Pr(NO_3)_3.xH_2O$, or $Gd(NO_3)_3.xH_2O$), 0.1 N NaOH was added drop wise and the solution was stirred well. The solution of **L1H** or **L2H** was added to this solution drop wise and the resulting solution was allowed to slowly evaporate to give light yellow crystals for **4**, green colour crystals for **6** and colourless crystals for rest of complexes within 1 week (70-73 % yield). M.p.>300 ºC.

Anal. Calcd for **NdL1 (1)**, $C_{21}H_{15}N_6O_{21}Nd$ (%): C, 30.33; H, 1.83; N, 10.11; Found: C, 30.34; H, 1.81; N, 10.20. IR (cm^{-1}) selected bonds: ν = 3579 (b) (O-H), 3082 (m) (Ar-H), 1639(w) $(COO^-)_{asy}$, 1535 (s) $(COO^-)_{sy}$, 1412 (w) (C=C), 1346 (m) (N-O), 589 (w) (M-O).

Anal. Calcd. For **EuL1 (2)**, $C_{21}H_{15}N_6O_{21}Eu_1$ (%): C, 30.03; H, 1.80; N, 10.46; Found: C, 30.05; H, 1.81; N, 10.70. IR (cm^{-1}) selected bonds: ν = 3557 (b) (O-H), 1622 (w) $(COO^-)_{asy}$, 1539 (s) $(COO^-)_{sy}$, 1415 (w) (C=C), 1342 (m) (N-O), 525 (w) (M-O).

Anal. Calcd for **NdL2(ac) (3)**, $C_{16}H_{13}N_4O_{16}Nd$ (%): C, 29.3; H, 1.98; N, 8.46; Found: C, 28.95; H, 1.91; N, 8.30. IR (cm^{-1}) selected bonds: ν = 3575 (b) (O-H), 3112 (m) (Ar-H), 1630 (s) $(COO^-)_{asy}$, 1539 (s) $(COO^-)_{sy}$, 1406 (m) (C=C), 1349 (m) (N-O), 583 (m) (M-O).

Anal. Calcd for **SmL2 (4)**, $C_{42}H_{18}N_{12}O_{40}Sm_2$ (%): C, 30.77; H, 1.60; N, 10.25; Found: C, 30.95; H, 1.81; N, 10.30. IR (cm^{-1}) selected bonds: ν = 3380 (b) (O-H), 1621 (w) $(COO^-)_{asy}$, 1542 (s) $(COO^-)_{sy}$, 1403 (w) (C=C), 1351 (m) (N-O), 578 (w) (M-O).

Anal. Calcd for **CeL2 (5)**, $C_{42}H_{24}N_{12}O_{40}Ce_2$ (%): C, 31.16; H, 1.62; N, 10.38; Found: C, 31.15; H, 1.67; N, 10.36. IR (cm^{-1}) selected bonds: ν = 3456 (b) (O-H), 1640 (m) $(COO^-)_{asy}$, 1536 (s) $(COO^-)_{sy}$, 1392 (m) (C=C), 1344 (m) (N-O), 532(w), 723 (s) (M-O).

Anal. Calcd for **PrL2 (6),** $C_{42}H_{18}N_{12}O_{40}Pr_2$ (%): C, 31.13; H, 1.62; N, 10.39; Found: C, 31.15; H, 1.65; N, 10.36. IR (cm^{-1}) selected bonds: ν = 3453 (b) (O-H), 1630 (m) $(COO^-)_{asy}$, 1541 (s) $(COO^-)_{sy}$, 1405 (m) (C=C), 1344 (m) (N-O), 517(w), 724 (s) (M-O).

Anal. Calcd for **LaL2 (7),** $C_{45}H_{31}N_{13}O_{40}La_2$ (%): C, 32.33; H, 1.86; N, 10.89; Found: C, 32.35; H, 1.87; N, 10.86. IR (cm^{-1}) selected bonds: ν = 3352 (b) (O-H), 1621 (m) $(COO^-)_{asy}$, 1538 (s) $(COO^-)_{sy}$, 1390 (m) (C=C), 1343 (m) (N-O), 529(w), 723 (s) (M-O).

Anal. Calcd for **EuL2 (8)**, $C_{42}H_{30}N_{12}O_{42}Eu_2$ (%): C, 30.03; H, 1.85; N, 10.46; Found: C, 30.05; H, 1.81; N, 10.30. IR (cm^{-1}) selected bonds: ν = 3586 (b) (O-H), 3108 (m) (Ar-H), 1630 (w) $(COO^-)_{asy}$, 1531 (m) $(COO^-)_{sy}$, 1435 (w) (C=C), 1352 (m) (N-O), 567 (w) (M-O).

Anal. Calcd for **GdL2 (9),** $C_{42}H_{30}N_{12}O_{42}Gd_2$ (%): C, 29.86; H, 1.85; N, 9.96; Found: C, 29.85; H, 1.81; N, 9.90. IR (cm^{-1}) selected bonds: ν = 3337 (b) (O-H), 3063 (m) (Ar-H), 1654 (w) $(COO^-)_{asy}$, 1548 (s) $(COO^-)_{sy}$, 1417 (w) (C=C), 1353 (m) (N-O), 625 (w) (M-O).

Anal. Calcd for **GdL2ac (10)**, $C_{22}H_{26}N_4O_{24}Gd_2$ (%): C, 24.93; H, 2.85; N, 5.46; Found: C, 24.95; H, 2.81; N, 5.30. IR (cm^{-1}) selected bonds: ν = 3339 (b) (O-H), 3064 (m) (Ar-H), 1658 (w)

$(COO^-)_{asy}$, 1546 (s) $(COO^-)_{sy}$, 1415 (w) (C=C), 1352 (m) (N-O), 622 (w) (M-O). (b = broad, m = medium, s = strong, w = weak).

X-ray crystallography

X-ray data of all these complexes were collected on a Bruker's Apex-II CCD diffractometer using Mo Kα (λ = 0.71069 Å) at room temperature except complexes **2** and **10** which are done at low temperature (100 K). The data collected by CCD diffractometer were processed by SAINT. Lorentz and polarization effects and empirical absorption corrections were applied using SADABS from Bruker. The structures were solved by direct methods, using SIR-92[70] and refined by full-matrix least squares refinement methods[71] based on F^2, using SHELX-2017. All non-hydrogen atoms were refined anisotropically. All hydrogen atoms were fixed geometrically with their U_{iso} values 1.2 times of phenylene carbons. The hydrogen atoms of water molecules were located from the difference Fourier synthesis (except for **4** and **6** which could not be) and were refined isotropically with distance of 0.82 Å with U_{iso} values 1.2 times that of their carrier oxygen atoms. The disorder in the nitro groups of **L2** in **4, 8** and **9** was resolved by splitting each of the affected atoms in two parts (using PART) with their site occupancy factors and U_{iso} values refined as free variables and constraints on their distances. In complex **7**, hydrogen atoms of methyl groups of coordinated DMF solvent were fixed geometrically with their U_{iso} values 1.5 times of their carrier carbons.

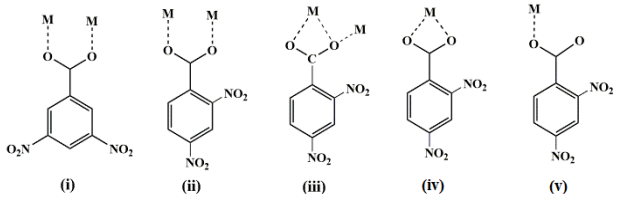

Scheme 1. Coordination modes observed, (i) (μ_2-κ^2, η^1: η^1) (ii) (μ_2-κ^2, η^1:η^1),(iii) (μ_2-κ^3, η^1:η^2) (iv) (μ_1-κ^2, η^1:η^1) (v) monodentate;

In complexes **3** and **10**, hydrogen atoms of methyl groups of coordinated acetate group were fixed geometrically with their U_{iso} values 1.5 times of their carrier carbons. Almost all structures show some residual peaks very close to the Ln(III) ion which may be due to the series termination error because of the heavy elements. All calculations were performed using WinGX package.[72] Crystal data and structure refinements for complexes **1**-**10** are given in Table S1. The important H-bonding parameters and bond parameters around the coordination sphere are given as supplemental material in Tables S2 and S3, respectively.

Results and Discussion

Crystal structure of 4*f*-block lanthanide ions based 1D complexes

$\{[Ln(\mu_2\text{-}L1)_3.(H_2O)_2].H_2O\}_n$ (Ln = Nd (III), Eu (III)). Both complexes are isomorphous hence only **NdL1 (1)** is described (Fig. 1 and S1) and the corresponding figures for **EuL2 (2)** complex and H-bonding discussion for complex **1** are given in supplementary (Fig S2-S4). **1** crystallises in triclinic space group Pī (Table S1). Its asymmetric unit contains one crystallographically independent Nd(III) ion, three **L1** anions, two coordinated water molecules and one water molecule present in lattice. The geometry around Nd(III) ion is bicapped trigonal prismatic (Fig. 1a) with six sites occupied by carboxylate oxygen atoms (O1, O2, O7, O8, O13 and O14) of **L1** and the remaining two sites by the oxygen atoms (O2W and O3W) of the water molecules. The average Nd-O bond length is 2.433(2) Å, which is comparable to those reported earlier for other Ln(III)-O complexes[73-78] and average Nd-Ow bond length is 2.546(2) Å.

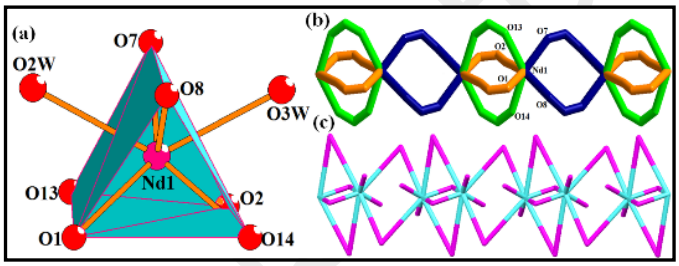

Fig 1. (a) Trigonal bicapped geometry around Nd(III) metal ion in complex **1**, (b) **L1** bridged paddle wheel dimeric units (green and orange colour) further bridged by **L1** (blue colour), forming linear tapes along *a* axis, (c) [1 0 0] chains of **1** with 2-connected uninodal net.

Four carboxylate groups from four centrosymmetric **L1** ligands coordinate two Nd(III) in mode (i) (Scheme 1), with *syn-syn* and *syn-anti* conformations[80] to form paddle wheel type centrosymmetric dimers (Fig 1b) . The successive dimeric units are further bridged by two centrosymmetric **L1** ligands, again in mode (i), with *syn-syn* conformation. The dihedral angles between two Nd-OCO planes in the dimer with Nd-OCO plane in this bridging link are 45.05(8)° and 45.16(5)°, forming twisted ribbons parallel to *a* axis. The two intrachain Nd···Nd distances are 4.245 Å and 5.102 Å, respectively. From a topological perspective,[80] this structure consists of [1 0 0] chains with a 2-connected uninodal net (Fig 1c) .

$[Nd(\mu_2\text{-}L2)_2.(CH_3COO).(H_2O)_2]_n$ (3). A room temperature synthesis of the earlier reported complex[60] shows supramolecular isomerism yielding a polymorph of the same complex as **3**. This complex crystallizes in triclinic centrosymmetric space group *P*ī (Table S1) having only one crystallographically independent $[Nd(\mu_2\text{-}\mathbf{L2})_2.(CH_3COO)(H_2O)_2]_n$ molecule in the unit cell (Fig. S5). Complex **3** differs from earlier reported complex[60] in terms of mode of coordination of **L2** with both ions bridging between the metal ions. Each Nd(III) metal ion occupies trigonal prismatic tricapped geometry with nine coordinating sites (Fig 2a). Here, four sites occupied by oxygens of carboxylate group, three sites by acetate oxygens, and two sites by water molecules (Fig 2b), form a twisted ribbon of 1D polymeric chain along *a* axis (Fig 2c). The coordination mode (ii) (Scheme 1) poses *syn-anti* and *syn-syn* conformations.[80] The carboxylate oxygens of **L2** are bridging between two Nd(III) ions and in case of acetate group, one oxygen atom is showing monodentate binding (Nd1-O14 2.573(19) Å) while other is in bidentate bridging mode (Nd1-

O13$^{\#1}$ 2.421(1) Å (#1: -x+2,-y+1,-z)). Two coordinated water molecules O1W and O2W are almost present in *trans* position with respect to chelating and bridging acetate groups. The Nd(III) metal ion are coordinating with **L2** ligands in monodentate fashion through O1, O2, O7 and O8 atom of carboxylate group with distance of Nd1-O1 = 2.440(2), Nd1-O2$^{\#1}$ = 2.474(2) (#1: -x+1, -y+2,-z), Nd1-O7 = 2.484(2) and Nd1-O8 = 2.453(2) Å.

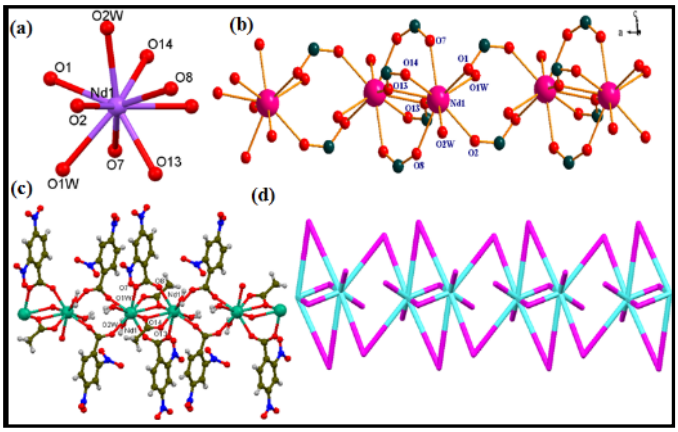

Fig 2. Showing for complex **3** (a) trigonal prismatic tricapped geometry around Nd(III) ion, (b) ball-n-stick representation showing coordination environment around Nd(III) ions, (c) ball-n-stick representation of 1D polymeric complex **3**, along *a* axis, (d) topologically, structure consists of [1 1 0] chains with 2-c uninodal net.

Nd-O(water) distance is in the range of 2.488(2) to 2.536(2) Å.. Topologically, [80] structure consists of chains [1 1 0] with 2-connected uninodal net (Fig 2d).

$[Ln_2(\mu_2\text{-}L2)_5.(L2).(H_2O)_4]_n$ (Ln = Sm (4), Ce (5), Pr (6). Complexes **4**, **5** and **6** are isomorphous and only a detailed structural description is given for **4.** The corresponding figures for complex **5** and **6** are given in supplementary **(**Fig S7-S8).

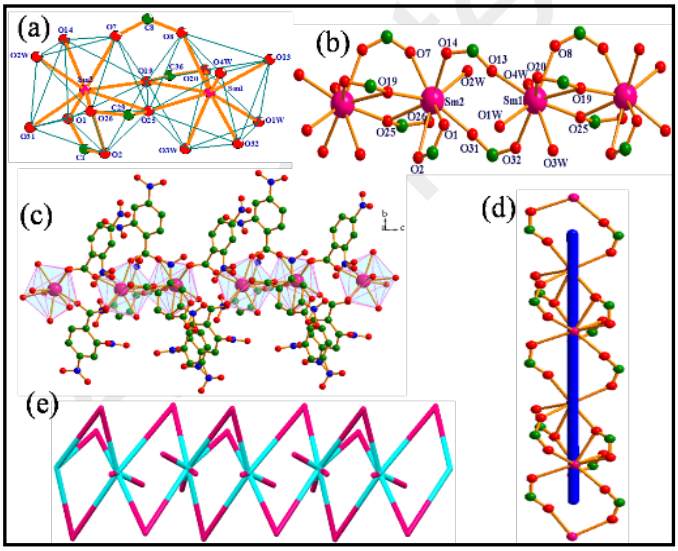

Fig 3. Showing (a) nanocoordinated distorted monocapped square-antiprism geometry around Sm(III) metal ion in complex **4**, (b) ball-n-stick representation of coordination environment around Sm(III) metal ions forming linear chain, (c) polyhedral representation of 1D coordination polymer along *c* axis, (d) 1D helical chain is formed showing down the *c* axis, (e) the chains [0 0 1] with 2-connected uninodal net.

Complex **4** crystallises in monoclinic, noncentrosymmetric space group *Cc* (Table S1). Its asymmetric unit contains two Sm(III) ions Sm1 and Sm2), six **L2** anions and four coordinated water molecules (Fig. S6). As shown in Fig 3a, complex **4** is a 1D coordination polymer where Sm1 and Sm2 are in nonacoordinated, distorted monocapped square-antiprism geometry. In this polymeric complex, all carboxylic groups are deprotonated and **L2** ligands display three types of binding modes(ii), (iii), and (iv) (Scheme 1). For Sm1, three sites are occupied by water molecules (O1W, O3W and O4W), with average bond distance 2.519(8) Å and remaining six sites by carboxylate oxygen atoms O8, O13, O19, O20, O25 and O32 of **L2** with average distance of Sm-O 2.454(8) Å. For Sm2, eight sites are occupied by carboxylate oxygen atoms O1, O2, O7, O14, O19, O25, O26 and O31 with average distance of Sm-O bonds 2.454(8) Å and one site by coordinated water molecule with distance Sm2-O2W = 2.489(8) Å (Fig 3b). One carboxylate group from **L2** ligand is forming bidentate bridge and two carboxylate groups from other **L2** ligands are showing chelating and bidentate bridging between two adjacent crystallographically equivalent Sm(III) ions in *syn-syn* and *syn-anti* conformations[80] with Sm···Sm distance 4.209(2) Å .These dimeric units are further connected by bidentate bridges of carboxylate groups from another **L2** ligand in *syn-syn* conformation with Sm···Sm distance of 5.047(2) Å, forming an infinite helical chain along *c* axis (Fig 3(c-d)). The hydrogen atoms of all four coordinated water molecules could not be located so main H-bonding interactions are between protons of aromatic ring and oxygen atoms of nitro groups forming an interesting 3D structure. From a topological perspective,[80] this structure consists of [0 0 1] chains with 2-connected uninodal net and 2C1 topological type (Fig 3e).

$[La_2(\mu_2\text{-}L2)_6.(H_2O)_3.(DMF)]_n$ (7). This complex crystallises in triclinic space group *P*$\bar{1}$ (Table S1). The asymmetric unit of this complex contains two La(III) ions, six **L2** anions, three coordinated water molecules and one coordinated dimethylformamide molecule (Fig. S9). Both La(III) ions are showing distorted bicapped square antiprismatic geometry with ten coordination sites (Fig 4a). La1 ion is coordinated by eight oxygen atoms from carboxyl group belonging to six **L2** molecules, and two water molecules. While La2 ion is coordinated by eight oxygen atoms from carboxyl group belonging to six **L2** molecules, one oxygen atom of dimethylformamide and one water molecule (Fig 4b). Each La(III) ion links to another adjacent La(III) ion by three carboxyl groups of three different **L2** ligands through bidentate and bridging bidentate mode of binding, with *syn-syn* and *syn-anti* conformations. The coordination modes of this complex are (ii) and (iii) (See Scheme 1) giving 1D polymeric chain along *a* axis. The strong intramolecular H-bonding interactions (Fig. S10) between coordinated water, DMF molecule and nitro group further support the 1D CP (Fig 4c).

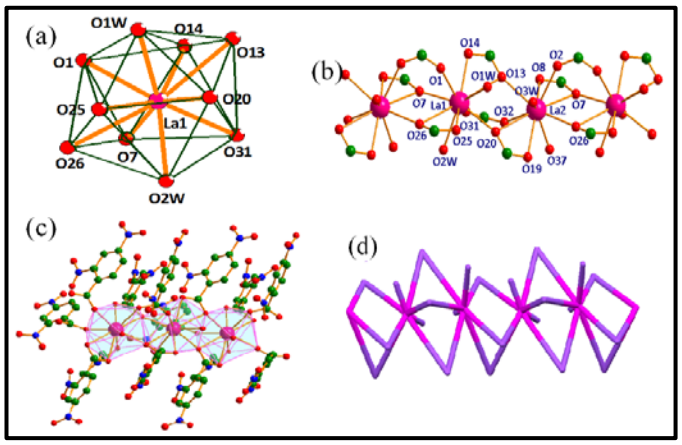

Fig 4. Showing (a) distorted bicapped square-antiprismatic geometry around La(III) metal ion in complex **7**, (b) ball-n-stick representation of coordination environment around La(III) metal ions forming linear chain, (c) polyhedral representation of 1D polymeric complex along *a* axis, (d) topological type: 2C1 with 2-c uninodal net.

The La1···La2 and La2···La1 distances are 4.484(3) and 4.522(3) Å, respectively. Topologically, [80] structure consists of 2-connected uninodal net with 2C1 topological type (Fig 4d).

Crystal structures of 4*f*-block transition metal ions based dimeric complexes

$[Ln(\mu_2\text{-}L2)_2.(L2).(H_2O)_3]_2$ (Ln = Eu (8), Gd (9)).

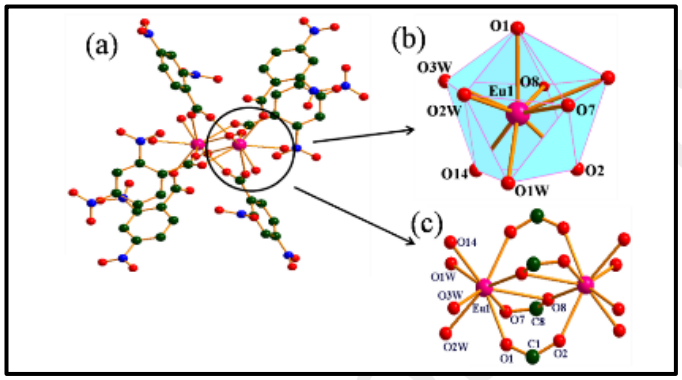

Fig 5. Showing (a) dimeric unit of complex **8**, (b) distorted monocapped square-antiprismatic, (c) coordination around Eu(III) ions,

Complexes **8** and **9** are isomorphous and isostructural, which crystallise in triclinic space group Pī (Table S1), so only one of them has been discussed and the corresponding figures for EuL2 (2) complex and H-bonding discussion for complex **8** are given in supplementary(Fig S11-S13). Complex **8** is having one Eu(III) ion, three **L2** ligands and three coordinated water molecules O1W, O2W and O3W in the unit cell (Figs 5a). A distorted monocapped square-antiprismatic geometry around Eu(III) ion (Fig 5b) has six sites occupied by oxygens of carboxylate group and three sites by oxygens of water molecules (Fig 5c). The coordination modes of this complex are (ii), (iii), and monodentate (v) (Scheme 1) with *syn-syn* and *syn-anti* conformations.[80] **L2** ligands are forming bidentate bridge between two Eu(III) ions through O1 and O2 oxygen atoms with bond distances Eu1-O1 = 2.394(4) Å, Eu1-O2#1 = 2.384(4) Å (#1: -x+2,-y,-z+2). The other two **L2** ligands are showing chelating and bidentate bridging between two Eu(III) ions through O7 and O8 oxygen atoms with bond distances Eu1-O7 = 2.524(4) Å, Eu1-O8 = 2.489(4)Å (average distance), whereas oxygen atom O14 of other **L2** ligand shows monodentate binding with Eu(III) ion with distance of Eu1-O14 = 2.359(5) Å. Three water coordinate with average distance of Eu1-OW = 2.416(4) Å and Eu1···Eu1#1 is 4.125(1) Å (#1: -x+2,-y,-z+2). Topologically,[80] the complex is 1M2-1 type with 1-connected uninodal net.

$[Gd(L2).(CH_3COO)_2.(H_2O)_2]_2$ (10). It is a simple dimeric complex, crystallising in orthorhombic centrosymmetric space group *Pbca* (Table S1). There is one crystallographically independent Gd(III) ion, one **L2** ligand, two acetate anions and two coordinated water molecules O1W and O2W in the unit cell (Figs 6a and S14). Each Gd(III) ion is nonacoordinated, having a distorted monocapped square antiprismatic geometry (Fig 6b) Only chelating mode of binding of **L2** ligand (iv) (Scheme 1) is present in this case with Gd1-O1 = 2.510(2) Å, Gd1-O2 = 2.484(2) Å. There are two types of acetate groups depending upon mode of coordination, chelating and bridging bidentate. The oxygens of one acetate group are chelating with one Gd(III) ion while the other one is bidentate bridging between two Gd(III) ions, with average Gd-O bond distance ca. 2.457(2) Å. Two water molecules coordinate with Gd1-O1W = 2.368(2) Å, Gd1-O2W = 2.363(2) Å and Gd···Gd non-bonding distance is 4.131(5) Å. H-bonding discussion for complex **10** are given in supplementary (Fig.S15)

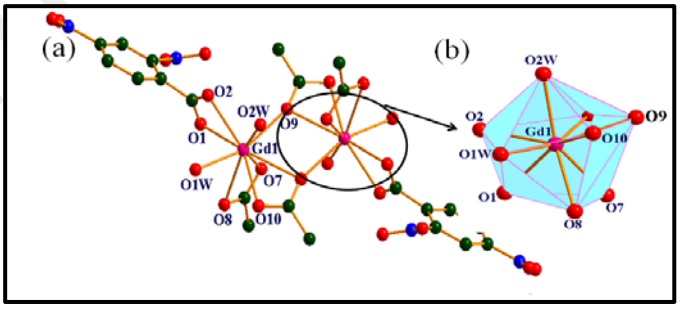

Fig 6. Showing (a) dimeric unit of complex **10**, (b) nanocoordinated distorted monocapped square-antiprismatic geometry,

. Topologically,[80] the complex is 1M2-1 type with 1-connected uninodal net.

IR Spectroscopy

All complexes **1**-**10** have been studied by IR spectroscopy. The expected symmetric and anti-symmetric –OH stretching bands, C-H and –C=C vibrations, symmetric and anti-symmetric stretches of COO-, aromatic N-O stretch and Ln-O vibrations have been identified and discussed in supporting information (Fig S16).

Powder X-ray Diffraction studies

In order to confirm that the single crystal structure of complexes **1**-**10** corresponds to the bulk material as well as its phase purity, the powder X-ray data were recorded at room

temperature. The experimental and simulated (from the single crystal data) patterns shown in supporting information (Figs. S17-S26), provide reasonably good match indicating that the single crystal and bulk material are the same.

Thermogravimetric analysis

The thermal stability of complexes **1**-**10** was examined by TGA (Fig. S27). The detailed analysis is available in the supporting information. In a general manner, the complexes highlighted successive endothermic peaks due to loss of lattice, coordinated solvent molecules and acetate anions, respectively. Then a sharp exothermic peak is observed due to the decomposition of the remaining metal molecular skeleton. Such decomposition happens in a temperature range of 244-420 °C depending of the number of bridging ligands and the nature of the lanthanide ions.

Photophysical Properties

Visible emissive properties

$\{[Eu(\mu_2\text{-}L1)_3.(H_2O)_2].H_2O\}_n$ (2) and $[Eu(\mu_2\text{-}L2)_2.(L2).(H_2O)_3]_2$ (8). The lanthanide coordination polymers may possess excellent luminescent properties in terms of their line-like and high colour-pure emissions.[33,81-83] Hence, the solid-state luminescent properties of lanthanide complexes are investigated at room temperature.

Photophysical properties of the **EuL1 (2)** complex have been measured in the solid state upon photoexcitation at 394 nm, which correspond to direct irradiation of the f-f transitions. Two intense bands at 613.5 and 618.5 nm arising from the $^5D_0 \rightarrow {}^7F_2$ transition have been recorded (Fig. 7). The four other expected contributions corresponding to transitions from the $^5D_0$ state to the $^7F_0$, $^7F_1$, $^7F_3$, and $^7F_4$ levels are also observed at 579, 592.5, 651.5 and 699 nm (band maxima), respectively.[84-85]

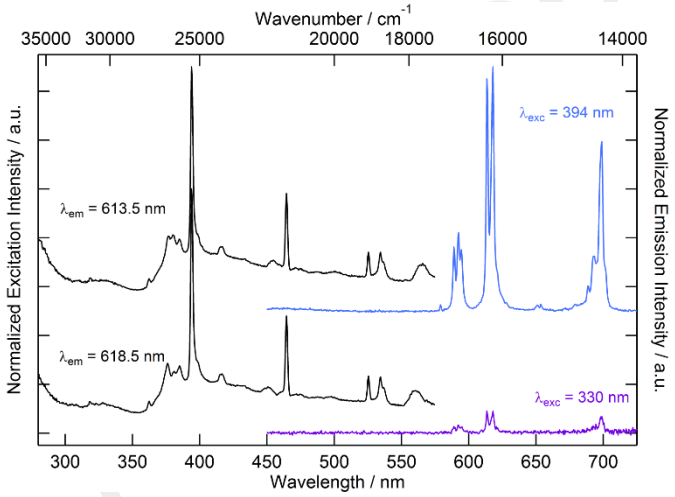

Fig 7. Solid-state excitation (black line) and emission spectra of **2** at room temperature (λ_{ex} = 394 nm, blue curve and λ_{ex} = 330 nm, purple curve). The intensities have been normalized on the more intense band at 394 nm and at 618.5 nm for the excitation and emission spectra, respectively.

Irradiation of **2** at lower wavelength (330 nm) produces a low intensity emission (Fig. 7) highlighting that the 3,5-dinitrobenzoate anion cannot play the role of organic chromophore in the sensitization of the Eu(III) luminescence. The energy transfer from the ligand to the Eu(III) is not efficient. It is known that the $^5D_0 \rightarrow {}^7F_2$ transition induced by the electric dipole moment is hypersensitive to the coordination environment of the Eu(III) ion, whereas the $^5D_0 \rightarrow {}^7F_1$ transition is magnetic dipole in origin and less sensitive to this feature. The $^5D_0 \rightarrow {}^7F_2$ transition is responsible for the red emission colour of **2** and its splitting is equal to 2 (Fig. 8) in agreement with the quite regular bicapped trigonal prismatic polyhedron.[86-87] As for **2**, the direct irradiation of the f-f transitions leads to a very intense red colour emission (Fig. 8).

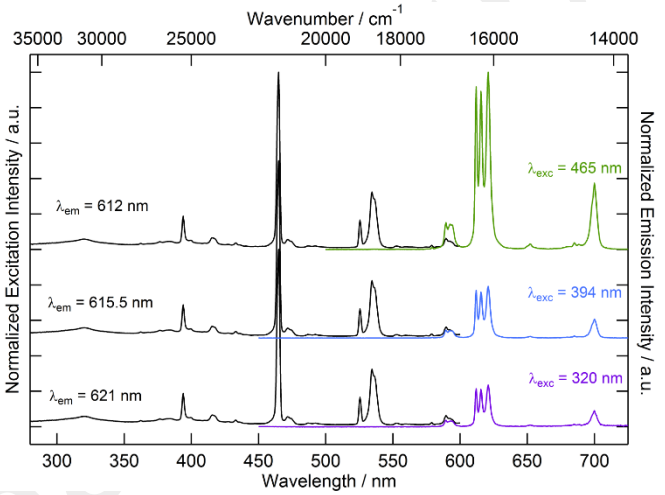

Fig 8. Solid-state excitation (black curve) and emission spectra of **8** at room temperature (λ_{ex} = 465 nm, green curve; λ_{ex} = 394 nm, blue curve and λ_{ex} = 330 nm, purple curve). The intensities have been normalized on the more intense band at 465 nm and at 621 nm for the excitation and emission spectra, respectively.

The second **EuL2 (8)** complex has been measured in the same experimental conditions upon photoexcitation at 465, 394 and 320 nm . Nevertheless two differences are observed: firstly irradiation of **8** at 320 nm induces a more efficient, but still weak sensitization by antenna effect when compared to **2**. It seems then that the 2,4-dinitrobenzoate anion is a more adapted chromophore for Eu(III) sensitization than the 3,5-dinitrobenzoate anion. Additionally the splitting of the $^5D_0 \rightarrow {}^7F_2$ transition is three instead of two, once more in agreement with the distorted monocapped square-antiprismatic geometry around the Eu(III) ion in **8**.

Near Infrared emissive properties

$\{[Nd(\mu_2\text{-}L1)_3.(H_2O)_2].H_2O\}_n$ (1) and $[Nd(\mu_2\text{-}L2)_2.(CH_3COO).(H_2O)_2]_n$ (3). The near-infrared luminescence of complexes **1** and **3** has also been investigated in the solid-state at room temperature. Irradiation of the f-f excitations gives a very weak, $^4F_{3/2} \rightarrow {}^4I_{11/2}$ emission of the Nd(III) ion (Figs S28 and S29) for both complexes. Irradiation at 330 nm shows an absence, in the case of **1** or a weak sensitization, in the case of **3,** by antenna effect. As observed on the Eu(III) derivatives the 2,4-dinitrobenzoate anion seems to be a more efficient antenna ligand than the 3,5-dinitrobenzoate anion.

$[Ln_2(\mu_2\text{-}L2)_5.(L2).(H_2O)_4]_n$ (Ln = Ce (5) and Pr (6)). No emission of the Ce(III) either Pr(III) ion for **5** and **6** has been observed upon photoexcitation at 381 and 330 nm (Fig. S30).

Magnetic Properties

Static magnetic measurements. The room temperature values of $\chi_M T$, with T the temperature in Kelvin and χ_M the molar magnetic susceptibility, are equal to ≅ 1.53 cm^3 K mol^{-1} for compounds **NDL1 (1)** and **NdL2ac (3)**. This is relatively in good agreement with the expected value (1.64 cm^3 K mol^{-1}) for the $^4I_{9/2}$ multiplet ground state. $\chi_M T$ decreases continuously on cooling to reach 0.55 and 0.66 cm^3 K mol^{-1} for **1** and **3** respectively at 2 K (Fig. S31). Both curves are almost perfectly superimposed except at very low temperature. It indicates that slightly different Stark sublevels are stabilized by ligand field/symmetry surroundings made by **L1** and **L2** and that the Kramers ground state doublet features different combination of M_J's. This is confirmed by the field dependence of the magnetization at 2 K which saturates at higher magnetic moment for **3** than for **1** (Fig. S31).

The temperature dependence of $\chi_M T$ for compound **EuL1 (2)** is represented on Fig. S32. $\chi_M T$ is equal to 1.37 cm^3 K mol^{-1} while the ground state $^7F_0$ is formally diamagnetic. This is due to the thermal population of spin-orbit states ^7F_J with J integer from 1 to 6. The analytical expression of the thermal variation of the magnetic susceptibility is given in Supporting Information. An excellent agreement between experiment and theory is obtained for λ = + 342 cm^{-1} (Fig. S32) with λ being the spin-orbit coupling constant). The magnetic behaviour of compound **EuL2 (8)** is equivalent to compound **EuL1 (2)** except that there are two metal sites per chemical units. The best agreement between experiment and theory is obtained for λ = +368 cm^{-1} (Fig. S33), similar to **2**.

An equivalent methodology can be applied to compound **SmL2 (4)**. The room temperature value of $\chi_M T$ is equal to 0.75 cm^3 K mol^{-1} and decreases continuously on lowering the temperature to reach 0.061 cm^3 K mol^{-1} at 2 K (Fig. S34). For the $^6H_{5/2}$ multiplet ground state the value expected for two Sm(III) should be close to 0.18 cm^3 K mol^{-1} ($g_{5/2}$ = 2/7) in the limit of the free ion model. However, like for Eu(III) complex, thermal population of higher multiplets (J = 7/2 to 15/2) induces deviation from the free ion model at high temperature.[88] At low temperature, crystal field effects and/or antiferromagnetic coupling between metal sites can explain the low value measured. Nevertheless, at higher temperatures than 150 K, the experimental $\chi_M T$ vs. T curve can be fairly well reproduced with a model (see supporting information for details) including all the multiplets contained in the ^6H ground term. The best agreement is obtained with λ = +245 cm^{-1} (Fig. S34).

The temperature dependence of $\chi_M T$ for compound **CeL2 (5)** is represented on Fig. S35. The room temperature value (0.7 cm^3 K mol^{-1}) is slightly lower than expected (0.8 cm^3 K mol^{-1}) for the uncoupled $^2F_{5/2}$ multiplet ground state. $\chi_M T$ decreases continuously on cooling down to 0.33 cm^3 K mol^{-1} at 2 K (Fig. S35). The field variation of the magnetization at 2 K reveals that the magnetization does not saturate with M = 0.65 Nβ under 50 kOe.

The temperature dependence of $\chi_M T$ for compound **PrL2 (6)** is represented on Fig. S36. The room temperature value is equal to 1.67 cm^3 K mol^{-1}, slightly higher than expected (1.6 cm^3 K mol^{-1}) for the $^3H_4$ multiplet ground state (Fig. S36). $\chi_M T$ decreases continuously on cooling down to 0.18 cm^3 K mol^{-1} at 2 K (Fig. S36). In a very interesting manner, χ_M tends to saturate at very low temperature (2K) (Fig. S36) which indicates a non-magnetic ground state due to crystal field effects.

For the last two compounds, namely **GdL2 (9)** and **GdL2ac (10)** , the room temperature values of $\chi_M T$ (15.73 and 15.64 cm^3 K mol^{-1} for **9** and **10**, respectively) are in excellent agreement with the expected (15.76 cm^3 K mol^{-1}) value for two uncoupled Gd^{III} spins ($^8S_{7/2}$) with *g* = 2.0 (Fig. S37). For both compounds, $\chi_M T$ remains constant down to 2K featuring the absence of sizable interactions between spins. At 2K, both field variations of the magnetization are easily reproduced with Brillouin function for two spins S = 7/2 with g = 1.99 and g = 1.98 for compounds **9** and **10** respectively.

Dynamic magnetic measurements. Compound **NDL1 (1)** and **NdL2ac (3)** show a frequency dependent signal below 7 K in the presence of an external dc field while all the other materials do not show any such dependence at any field and temperature. We decided to apply the same magnetic field that in our previous studies[60] to compare the results. A magnetic field of 2 kOe has been set for compound **1** and 3.5 kOe for **3**. These fields correspond to the slowest relaxation of the magnetic moment and both systems show typical SMM behaviour. The frequency dependences of both in-phase, χ_M', and out-of-phase, χ_M'', below 6 K are represented in Fig. 9 for **1** and **3**.

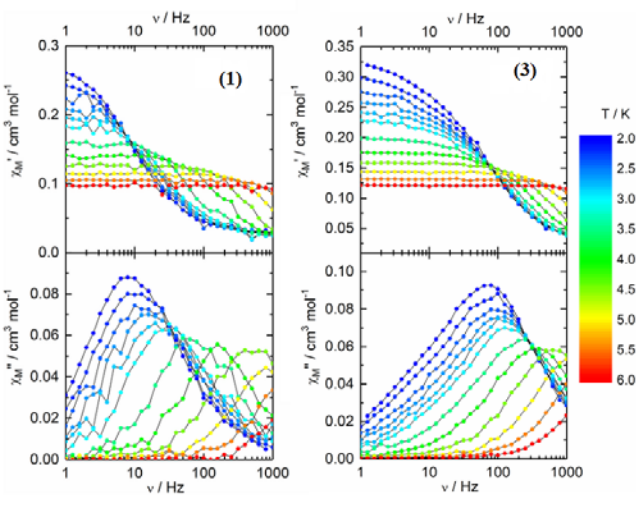

Fig 9. Frequency dependence of χ_M' (top) and χ_M'' (down) components of the ac susceptibility for **1** (on the left) and **3** (on the right) at various temperatures under an applied magnetic field of 2 kOe.

At each temperature the frequency variations can be analysed in the framework of the extended Debye model.[89-90]

$$\chi_M' = \chi_S + (\chi_T - \chi_S)\frac{1+(\omega\tau)^{1-\alpha}\sin\left(\alpha\frac{\pi}{2}\right)}{1+2(\omega\tau)^{1-\alpha}\sin\left(\alpha\frac{\pi}{2}\right)+(\omega\tau)^{2-2\alpha}}$$

$$\chi_M'' = (\chi_T - \chi_S)\frac{(\omega\tau)^{1-\alpha}\cos\left(\alpha\frac{\pi}{2}\right)}{1+2(\omega\tau)^{1-\alpha}\sin\left(\alpha\frac{\pi}{2}\right)+(\omega\tau)^{2-2\alpha}}$$

With χ_T the isothermal susceptibility, χ_S the adiabatic susceptibility, α the dispersion of the relaxation time τ and $\omega = 2\pi\nu$, with ν the frequency of the oscillating field. The best fitted values are given in Tables S4 and S5. For both compounds, **NDL1 (1)** and **NdL2ac (3)** , the distribution of the relaxation time is relatively narrow since it does not exceed 0.3. The high frequency limits of the magnetic susceptibility (χ_S) remain small which means that the relaxation concern the vast majority of the complexes and the low frequency limits match almost perfectly the dc regime. The temperature variations of the relaxation time for both compounds are given in Fig. 10. The thermal behaviour of the relaxation times can be analysed by the combination of a thermally activated process (Arrhenius) which dominates at high temperature and a thermally independent process which dominates at low temperature. The curves can then be reproduced with the following equation:

$$\tau^{-1} = \tau_0^{-1}\exp\left(-\frac{\Delta}{T}\right) + \tau_{TI}^{-1}$$

With τ_0 the intrinsic relaxation time, Δ the activation energy of the Arrhenius process and τ_{TI} the relaxation time of the thermally independent process, the best fits are obtained for **1** and **3** (in brackets) with τ_0 = 7.29(3)×10^{-7} s [3.43(2)×10^{-6} s], Δ = 28(2) K [19.7(2) K] and τ_{TI} = 0.014(2) s (0.0026(2) s).

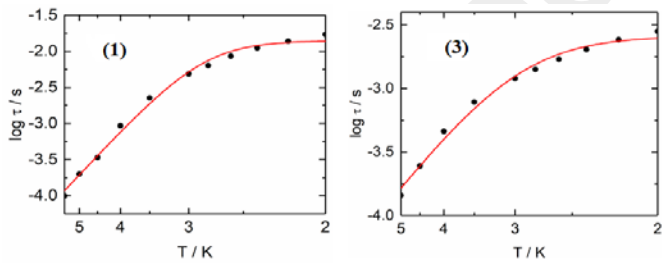

Fig 10. Temperature dependence of the relaxation time extracted with the help of the extended Debye model for **1** (on the left) and **3** (on the right). The red line corresponds to the best fitted curve with a modified Arrhenius law (see text).

Some of us have shown that the two polymers {[Nd(μ_2-**L1**)$_3$(H_2O)$_2$]·MeCN}$_n$ (MeCN= acetonitrile) and [Nd(μ_2-**L2**)(**L2**)(CH_3COO)(H_2O)$_2$]$_n$ displayed slow magnetic relaxation with respective energy activation of 27 K and 29 K.[60] In the present cases, **1** has an energy activation of 28 K which is very similar to {[Nd(μ_2-**L1**)$_3$(H_2O)$_2$]·MeCN}$_n$ demonstrating that the nature of the solvent of crystallisation has no effect on the dynamic magnetic properties. Whereas the polymorph **3** of the previously reported [Nd(μ_2-**L2**)(**L2**)(CH_3COO)(H_2O)$_2$]$_n$, relaxes faster and has a lower energy barrier (Δ = 19.7 K). It apparently demonstrates that the (terminal vs bridging) mode of coordination of the second **L2** ligand makes a significant difference in raising the energy barrier and slowing down the relaxation process.

Conclusions

In this work, we have reported ten complexes, using lanthanide ions with positional isomers **L1H** and **L2H** and studied them from the crystal engineering point of view. Their X-ray crystal structures unfold a plethora of coordination modes and supramolecular architectures. Commencing from 0D monomers and paddle-wheel dimers to linear 1D tapes, the nitro benzoates offer versatility, novelty and thermal stability in inorganic-organic hybrids. Combining our observations with those found in the literature it has been seen that the engineering of a particular architecture for these ligands depends on the conformation of the ligand, disposition and participation of –NO_2 groups and nature and size of the metal ion.

The visible Eu(III) luminescence could be observed for both compounds **EuL1 (2)** and **EuL2 (8)** by direct sensitization of the *f-f* transitions but not through an antenna effect. The NIR luminescence of the two Nd(III) analogues, was detected owing to a direct *f-f* sensitization in **NDL1 (1)** and a weak sensitization through antenna effect in case of **NdL2ac (3)** . In all cases, **L2** ligand seems to be a weak but better organic antenna than **L1**.

Finally, in addition to their luminescence, the two Nd(III)-based polymers **NDL1 (1)** and **NdL2ac (3)** highlighted slow relaxation of the magnetization under an optimal applied magnetic field making them one of the rare examples of Nd(III)-based luminescent compounds with SMM behaviour. The electronic distribution confers by the chemical surrounding is suitable to stabilize a strong anisotropy for Nd(III) while it is not for the other ions.

Few questions remain open on the difference between both ligands for the magnetic and optical properties. To quantitatively answer to these questions, computational calculations will be carried out to determine the excited energy states as well as the electronic distribution and the nature of the magnetic anisotropy for the different lanthanide ions in presence of L1 or L2.

Conflicts of interest

There are no conflicts to declare.

Acknowledgements

AKJ thanks Department of Science and Technology for INSPIRE fellowship for PhD. She is currently pursuing post-doctoral fellowship at Indian Institute of Technology Delhi, New Delhi, India. BSS thanks University Grants Commission(India) for BSR fellowship for Ph.D. GH thanks Council of Scientific and Industrial Research, India (research grant No. 01(2406)/10/EMR-II) and University Grants Commission(India)

for research grant under UPE (University with potential for excellence) scheme for GNDU, for financial assistance. This work was financially supported by Région Bretagne, Rennes Métropole, CNRS, Université de Rennes 1, FEDER and the ANR (ANR-13-BS07-0022-01).

Notes and references

1 O. Guillou and C. Daiguebonne, *Handbook on the Physics and Chemistry of Rare Earths (vol 34).*
2 K. A. Gschneider, J.-C. G. Bünzli, V. K. Pecharsky, Eds.; Elsevier 2005; Vol. 34; 359-404.
3 J.-C. G. Bünzli and C. Piguet, *Chem. Soc. Rev.,* 2005, **34**, 1048-1077.
4 L. J. Charbonnière, N. Hildebrandt, R. F. Ziessel and H.-G. Löhmannsröben, *J. Am. Chem. Soc.,* 2006, **128**, 12800-12809.
5 A. Datta and K. N. Raymond, *Acc. Chem. Res.,* 2009, **42**, 938-947.
6 S. Aime, D. D. Castelli, S. G. Crich, E. Gianolio and E. Terreno, *Acc. Chem. Res.,* 2009, **42**, 822-831.
7 J.-C. G. Bünzli, *Chem. Rev.,* 2010, **110**, 2729-2755.
8 K. Kuriki, Y. Koike and Y. Okamoto, *Chem. Rev.,* 2002, **102**, 2347-2356.
9 L.-M. Fu, X.-F. Wen, X.-C. Ai, Y. Sun, Y.-S. Wu, J.-P. Zhang and Y. Wang, *Angew. Chem., Int. Ed*., 2005, **44**, 747-750.
10 S. Suárez, D. Imbert, F. Gumy, C. Piguet and J.-C. G. Bünzli, *Chem. Mater*., 2004, **16**, 3257-3266.
11 C.-S. Liu, L.-F. Yan Z. Chang and J.-J. Wang, *Acta Crystallogr., Sect. E,* 2008, **64**, m15-m16.
12 C. Lampropoulos, T. C. Stamatatos, K. A. Abboud and G. Christou, *Inorg. Chem*., 2009, **48**, 429-431.
13 J.-C. G. Bünzli, *Acc. Chem. Res*. 2006, **39**, 53-61.
14 F. Pointillart, B. Le Guennic, O. Cador, O. Maury and L. Ouahab, *Acc. Chem. Res.*, 2015, **48**, 2834-2842.
15 H. Bubkamp, G. B. Deacon, M. Hilder, P. C. Junk, U. H. Kynast, W. W. Lee and D. R. Turner, *Cryst. Eng. Commun*., 2007, **9**, 394-411.
16 J.-W. Ye, J. Wang, J.-Y. Zhang, P. Zhang and Y. Wang, *Cryst. Eng. Commun*. 2007, **9**, 515-523.
17 B. H. Ye, M. L. Tong and X. M. Chen, *Coord. Chem. Rev*., 2005, **249**, 545-565.
18 S. G. Roh, M. K. Nah, J. B. Oh, N. S. Baek, K-M. Park and H. K. Kim, *Polyhedron,* 2005, **24**, 137-142.
19 S. Mukherjee, M. R. Daniels, R. Bagai, K. A. Abboud, G. Christou and C. Lampropoulos, *Polyhedron,* 2010, **29**, 54-65.
20 R. Shyni, S. Biju, M. L. P. Reddy, A. H. Cowley and M. Findlater, *Inorg. Chem.* 2007, **46**, 11025-11030.
21 S. Raphael, M. L. P. Reddy, A. H. Cowley, M. Findlater, *Eur. J. Inorg. Chem.,* 2008, 4387-4394.
22 X.-Y. Chen, C. Marchal, Y. Filinchuk, D. Imbert and M. Mazzanti, *Chem. Commun.,* 2008, **0**, 3378-3380.
23 X. Li, Z.-Y. Zhang and Y-Q. Zou, *Eur. J. Inorg. Chem.,* 2005, **14** 2909-2918.
24 Y. Li, F. K. Zheng, X. Liu, W. Q. Zou, G. C. Guo, C. Z. Lu and J. S. Huang, *Inorg. Chem.,* 2006, **45**, 6308-6316.
25 S. Sivakumar, M. L. P. Reddy, A. H. Cowley and K. V. Vasudevan, *Dalton Trans.,* 2010, **39**, 776-786.
26 A. R. Ramya, M. L. P. Reddy, A. H. Cowley and K. V. Vasudevan, *Inorg. Chem.,* 2010, **49**, 2407-2415.
27 M. Yin and J. Sun, *J. Alloys Compd.,* 2004, **381**, 50-57.
28 M.-C. Yin, C.-C. Ai, L.-J. Yuan, C.-W. Wang and J.-T. Sun, *J. Mol. Struct*., 2004, **691**, 33-37.
29 M.-X. Hu, Y.-G. Chen, C.-J. Zhang and Q.-J. Kong, *Cryst. Eng. Commun.,* 2010, **12**, 1454-1460.
30 D. N. Woodruff, R. E. P. Winpenny, R. A. Layfield, *Chem. Rev.,* 2013, **113**, 5110-5148.
31 B. D. Culiity, C. D. Graham, Introduction to Magnetic Materials, Jonh Wiley & Sons:Hoboken, NJ, 2008.
32 J. D. Rinehart, J. R. Long, *Chem. Sci.*, 2011, **2**, 2078.
33 M.-X. Hu, Y.-G. Chen, C.-J. Zhang and Q.-J. Kong, *Cryst. Eng. Commun*., 2010, **12**, 1454-1460.
34 D. N. Woodruff, R. E. P. Winpenny and R. A. Layfield, *Chem. Rev.*, 2013, **113**, 5110-5148.
35 H. L. C. Feltham and S. Brooker, *Coord. Chem. Rev.*, 2014, **276**, 1-33.
36 P. Zhang, Y.-N. Guo and J. Tang, *Coord. Chem. Rev.*, 2013, **257**, 1728-1763.
37 A. Caneschi, D. Gatteschi, N. Lalioti, C. Sangregorio, R. Sessoli, G. Venturi, A. Vindigni, A. Rettori, M. G. Pini and M. A. Novak, *Angew. Chem., Int. Ed.*, 2001, **40**, 1760–1763.
38 L. Bogani, C. Sangregorio, R. Sessoli and D. Gatteschi, *Angew. Chem., Int. Ed.*, 2005, **44**, 5817–5821
39 K. Bernot, L. Bogani, A. Caneschi, D. Gatteschi and R. Sessoli, *J. Am. Chem. Soc.,* 2006, **128**, 7947–7956
40 E. Bartolome, J. Bartolome, S. Melnic, D. Prodius, S. Shova, A. Arauzo, J. Luzon, F. Luis and C. Turta, *Dalton Trans.*, 2013, **42**, 10153-10171.
41 J. Jung, F. Le Natur, O. Cador, F. Pointillart, G. Calvez, C. Daiguebonne, O. Guillou, T. Guizouarn, B. Le Guennic and K. Bernot, *Chem. Commun.* 2014, **50**, 13346-13348.
42 Y.-M Song, F. Luo, M.-B. Luo, Z.-W. Liao, G.-M. Sun, X.-Z. Tian, Y. Zhu, Z.-J. Yuan, S.-J. Liu, W.-Y. Xu and X.-F. Feng, *Chem. Commun.*, 2012, **48**, 1006-1008.
43 D. T. Thielemann, A. T. Wagner, Y. Lan, C. E. Anson, M. T. Gamer, A. K. Powell and P. W. Roesky, *Dalton. Trans.*, 2013, **42**, 14794-14800.
44 Y.-B. Lu, X.-M. Jiang, S.-D. Zhu, Z.-Y. Du, C.-M. Liu, Y.-R. Xie and L.-X. Liu, *Inorg. Chem.* 2016, **55**, 3738-3749.
45 F. Pointillart, B. Le Guennic, S. Golhen, O. Cador, O. Maury and L. Ouahab, *Chem. Commun*., 2013, **49**, 615-617.
46 A. B. Castro, J. Jung, S. Golhen, B. Le Guennic, L. Ouahab, O. Cador and F. Pointillart, *Magnetochemistry* 2016, **2**, 26-37.
47 Y.-N. Guo, G.-F. Xu, P. Gamez, L. Zhao, S.-Y. Lin, R. Deng, J. Tang and H.-J. Zhang, *J. Am. Chem. Soc.*, 2010, **132**, 8538-8539.
48 Y.-N. Guo, G.-F. Xu, W. Wernsdorfer, L. Ungur, Y. Guo, J. Tang, H.-J. Zhang, L.F. Chibotaru and A.K. Powell, *J. Am. Chem. Soc.*, 2011, **133**, 11948-11951.
49 S.-Y. Lin, W. Wernsdorfer, L. Ungur, A.K. Powell, Y.-N. Guo, J. Tang, L. Zhao, L.F. Chibotaru and H.-J. Zhang, *Angew. Chem. Int. Ed.* 2012, **51**, 12767-12771.
50 Y.-N. Guo, L. Ungur, G. E. Granroth, A. K. Powell, C. Wu, S. E. Nagler, J. Tang, L. F. Chibotaru and D. Cui, *Sci. Rep.*, 2014, **4**, 5471-5477.
51 R. A. Layfield, *Organometallics*, 2014, **33**, 1084-1099.
52 Y.-N. Guo, G.-F. Xu, Y. Guo and J. Tang, *Dalton Trans.*, 2011, **40**, 9953-9963.
53 P. Zhang, L. Zhang and J. Tang, *Dalton Trans.*, 2015, **44**, 3923.
54 L. Ungur, S.-Y. Lin, J. Tang and L. F. Chibotaru, *Chem. Soc. Rev.,* 2014, **43**, 6894-6905.
55 J. J. Le Roy, I. Korobkov, J. E. Kim, E. J. Schelter and M. Murugesu, *Dalton Trans.* 2014, **43**, 2737-2740.
56 A. Ben Khélifa, M. Salah Belkhiria, G. Huang, S. Freslon, O. Guillou and K. Bernot, *Dalton Trans.*, 2015, **44**, 16458-16464.
57 J. J. Le Roy, S. I. Gorelsky, I. Korobkov and M. Murugesu, *Organomettalics*, 2015, **34**, 1415-1418.
58 J. D. Rinehart and J. R. Long, *Dalton Trans.*, 2012, **41**, 13572-13574.
59 J. J. Baldovi, J. M. Clemente-Juan, E. Coronado and A. Gaita-Arino, *Polyhedron*, 2013, **66**, 39-42.
60 A. K. Jassal, N. Aliaga-Alcalde, M. Corbella, D. Aravena, E. Ruiz and G. Hundal, *Dalton Trans.*, 2015, **44**, 15774.

61 H. Wada, S. Ooka, T. Yamamura and T. Kajiwara, *Inorg. Chem.*, 2017, **56**, 147-155.
62 F. Pointillart, O. Cador, B. Le Guennic and L. Ouahab, *Coord. Chem. Rev.* 2017, **346**, 150-175.
63 S. Hino, M. Maeda, K. Yamashita, Y. Kataoka, M. Nakano, T. Yamamura, H. Nojiri, M. Kofu, O. Yamamuro and T. Kajiwara, *Dalton Trans*., 2013, **42**, 2683–2686.
64 S. Hino, M. Maeda, Y. Kataoka, M. Nakano, T. Yamamura and T. Kajiwara, *Chem. Lett.*, 2013, **42**, 1276–1278.
65 S. K. Singh, T. Gupta, L. Ungur and G. Rajaraman, *Chem. – Eur. J.*, 2015, **21**, 13812–13819.
66 J. J. Baldoví, J. M. Clemente-Juan, E. Coronado, Y. Duan, A. Gaita-Ariño and C. Giménez-Saiz, *Inorg. Chem*., 2014, **53**, 9976–9980.
67 A. Arauzo, A. Lazarescu, S. Shova, E. Bartolome, R. Cases, J. Luzon, J. Bartolome and C. Turta,*Dalton Trans.,* 2014,**43**, 12342–12356.
68 S. K. Gupta, T. Rajeshkumar, G. Rajaraman and R. Murugavel, *Chem. Commun*., 2016, **52**, 7168-7171.
69 G. A. Bain and J. F. Berry, *J. Chem. Educ*., 2008, **85**, 532-536.
70 A. Altomare, G. Cascarano, C. Giacovazzo and A. Guagliardi, *J. Appl. Crystallogr.*, 1993, **26**, 343-350.
71 G. M. Sheldrick, *Acta Cryst*., *2015* **C71***. 3-8*.
72 L. J. Farrugia, *J. Appl. Cryst.*, 1999, **32**, 837-838.
73 S. S.-Y. Chui, S. M.-F. Lo, J. P. H. Charmant, A. G. Orpen and I. D. Williams, *Science* 1999, **283**, 1148-1150.
74 H. Li, M. Eddaoudi, M. O'Keeffe and O. M. Yaghi, *Nature*, 1999, **402**, 276-279.
75 N. L. Rosi, M. Eddaoudi, J. Kim, M. O'Keeffe and O. M.; Yaghi, *Cryst. Eng. Commun.*, 2002, **4**, 401-404.
76 D. Sun, D. J. Collins, Y. Ke, J. Zuo and H. Zhou, *Chem. Eur. J.*, 2006, **12**, 3768-3776.
77 H. Abourahma, G. J. Bodwell, J. Lu, B. Moulton, I. R. Pottie, R. B. Walsh and M. J. Zaworotko, *Cryst. Growth Des.*, 2003, **3**, 513-519.
78 A. C. Sudik, A. P. Cote and O. M. Yaghi, *Inorg. Chem.,* 2005, **44**, 2998-3000.
79 H. Arora and R. Mukherjee, *New J. Chem.*, 2010, **34**, 2357-2365.
80 V. A. Blatov, *IUCr Comp. Commun. Newsletter.* 2006, **7**, 4.
81 M. Watanabe, T. Nankawa, T. Yamada, T. Kimura, K. Namiki, M. Murata, H. Nishihara and S. Tachimori, *Inorg. Chem*., 2003, **42**, 6977-6979.
82 V. Patroniak, P. N. W. Baxter, J.-M. Lehn, Z. Hnatejko and M. Kubicki, *Eur. J. Inorg. Chem*., 2004, **43**, 2379-2386.
83 C.-B. Liu, C.-Y. Sun, L.-P. Jin and S.-Z. Lu, *New J. Chem*., 2004, **28**, 1019-1026.
84 Z.-H. Zhang, Y. Song, T. Okamura, Y. Hasegawa, W.-Y. Sun and N. Ueyama, *Inorg. Chem.*, 2006, **45**, 2896-2902.
85 X. Wang, Y. Guo, Y. Li, E. Wang, C. Hu and N. Hu, *Inorg. Chem.* 2003, **42**, 4135-4140.
86 L. D. Carlos and A. L. L. Videira, *Phys. Rev. B*, 1994, **49**, 11721-11728.
87 Y.-F. Liu, G.-F. Hou, Y.-H. Yu, P.-F. Yan, J.-Y. Li, G.-M. Li and J.-S. Gao, *Cryst. Growth Des*., 2013, **13**, 3816-3824.
88 O. Kahn, *Molecular Magnetism, VCH: Weinhem*, 1993.
89 C. Dekker, A. F. M. Arts, H. W. Wijn, A. J. van Duyneveldt and J. A. Mydosh, *Phys. Rev. B,* 1989, **40**, 11243-11251.
90 K. S. Cole and R. H. Cole, *J. Chem. Phys.,* 1941, **9**, 341-351.